

Pressure-induced enhancement of superconductivity and quantum criticality in the 12442-type hybrid-structure superconductor $\text{KCa}_2\text{Fe}_4\text{As}_4\text{F}_2$

Bosen Wang,^{1,2,5,*} Zhi-Cheng Wang,³ Kento Ishigaki,² Kazuyuki Matsubayashi,² Tetsujiro Eto,⁴ Jianping Sun,¹ Jin-Guang Cheng,^{1,5} Guang-Han Cao,³ and Yoshiya Uwatoko²

¹Beijing National Laboratory for Condensed Matter Physics and Institute of Physics, Chinese Academy of Sciences, Beijing 100190, China

²Institute for Solid State Physics, University of Tokyo, Kashiwanoha 5-1-5, Kashiwa, Chiba 277-8581, Japan

³Department of Physics and State Key Laboratory of Silicon Materials, Zhejiang University, Hangzhou 310027, China

⁴Faculty of Engineering, Kurume Institute of Technology, Kurume, Fukuoka 830-0052, Japan

⁵Songshan Lake Materials Laboratory, Dongguan, Guangdong 523808, China



(Received 4 July 2018; revised manuscript received 19 November 2018; published 2 January 2019)

We report a domelike superconductivity and quantum criticality in the 12442-type hybrid-structure superconductor $\text{KCa}_2\text{Fe}_4\text{As}_4\text{F}_2$ under hydrostatic pressures up to 15 GPa. It is found that the superconducting transition temperature (T_c) increases from ~ 33.5 K at ambient pressure to a maximum of ~ 36.5 K at 2 GPa in the background of enhanced resistivity of the (K, Rb, Cs) $\text{Ca}_2\text{Fe}_4\text{As}_4\text{F}_2$ at ambient pressure (AP), and then shows a slope change near 8 GPa with anomalous characteristics of resistivity. T_c is found to be inversely proportional to the characteristic temperature of the coherence-incoherence crossover. The plots of resistivity at various temperatures and pressures and high-pressure x-ray diffraction confirm no pressure-induced half collapse of the tetragonal structure below 15 GPa. The pressure-induced crossover from non-Fermi liquid (the temperature exponent $n \sim 1.05 \pm 0.1$ at AP) to Fermi liquid ($n \sim 1.92 \pm 0.1$ at 15 GPa) is accompanied by the reduction of the linear temperature coefficient of normal-state resistivity, nearly two orders of magnitude compared to AP. These characteristics are ascribed to the weakening electronic correlation and/or critical fluctuations by pressure.

DOI: [10.1103/PhysRevB.99.014501](https://doi.org/10.1103/PhysRevB.99.014501)

Recently, the hybrid structures, or the intergrowths, of FeAs-based superconductors (SCs) have been extensively studied [1–5]. Different from the previously reported solid solutions, the independent alkali-metal, alkaline-earth, and/or rare-earth ions are stacked orderly across the double Fe_2As_2 layers [1–3]. The resulting asymmetric Fe_2As_2 layers as well as the lengthening c axis and c/a ratio make their band structures and Fermi surfaces more complicated compared to other FeAs-based SCs [2,6]. Until now, 1144- and 12442-type hybrid structures have been reported by combining various 122- and/or 1111-type FeAs-based materials, which are usually low- T_c SCs and/or non-SCs [1–3,7,8]. At ambient pressure (AP), hybrid structures usually exhibit bulk superconductivity with higher T_c of ~ 30 – 37 K [1–5] and share many common features, e.g., multiband effect [6,9,10], unconventional superconductivity [11,12], and structural instability [4,13]. Especially, several rare-earth contained hybrid structures display unusual coexistence of ferromagnetism and superconductivity [3,13,14], providing a platform to study the interplay of structure, magnetism, and superconductivity.

The 12442-type hybrid structure is the intergrowth of 1111- and 122-type FeAs-based materials, e.g., CaFeAsF and (K, Rb, Cs) Fe_2As_2 [2,6]. The recently discovered $\text{KCa}_2\text{Fe}_4\text{As}_4\text{F}_2$ with $T_c \sim 33.2$ K is the very first example [2]. It consists of alternate stacking of the conducting Fe_2As_2 layers and insulating Ca_2F_2 -charge reservoir layers. Internal charge transfers between double Fe_2As_2 layers (from

CaFeAsF to KFe_2As_2) along with the change of Fe valence state, termed as self-doping, can explain its higher T_c [2,6,15]. Differently, the substitutions of Co for Fe can suppress the superconducting state with the loss of bulk SCs for the Co/Fe ratio over 1/3, when the dominant charge carriers change from p type to n type accompanied with the variation of Fermi surfaces. However, it was believed that the Co/Fe disorders rather than chemical pressure play an important role for suppressing the SC [5]. The absence of magnetic ordering here is inconsistent with the case of the Co/Ni-doped 1144-type $\text{KCaFe}_4\text{As}_4$ with spin-vortex crystal-type orderings [16]. In addition, a nodal multigapped SC has been proposed via the transverse-field muon spin rotation (μSR), similar to the cases of (Rb, Cs) $\text{Ca}_2\text{Fe}_4\text{As}_4\text{F}_2$ [10] and $\text{KCaFe}_4\text{As}_4$ [9]. Theoretical calculations also support the above scenario [6]. $\text{KCa}_2\text{Fe}_4\text{As}_4\text{F}_2$ is suggested to have multiband character with ten bands across the Fermi level and strong tendency towards the stripe antiferromagnetic order [6,17], which is suppressed by charge redistributions, and superconductivity emerges. These characteristics indicate that $\text{KCa}_2\text{Fe}_4\text{As}_4\text{F}_2$ is close to a quantum critical point (QCP) with enhanced critical fluctuations, and studies on high-pressure effect can deepen the understanding of the underlying physical mechanisms. The indirect effect of the alkali-metal element substitution in (K, Rb, Cs) $\text{Ca}_2\text{Fe}_4\text{As}_4\text{F}_2$ has been investigated and the results show that T_c decreases with increasing the lattice parameters a and c . In contrast, an opposite trend of T_c was observed in the 1144-type hybrid structures [2,18]. It is argued that the coupling strengths of the asymmetrical double Fe_2As_2 layers affect T_c in (K, Rb, Cs) $\text{Ca}_2\text{Fe}_4\text{As}_4\text{F}_2$ while

*bswang@iphy.ac.cn

in some oxygen-containing 12442-type hybrid-structure SCs the interlayer couplings and structural instability are thought to be more crucial to superconducting pairings [19]. Detailed studies have revealed that T_c is related to the c/a ratio of 12442-type SCs and tends to increase with enhanced lattice mismatch between CaFeAsF and KFe_2As_2 blocks [20]. However, the physical pressure effect has not been reported until now to our knowledge. In this regard, one interesting point is the pressure-induced collapse of tetragonal phase. $\text{KCa}_2\text{Fe}_4\text{As}_4$ undergoes first a half-collapsed tetragonal transition at ~ 4 GPa with the loss of bulk superconductivity, and then second a complete-collapsed tetragonal transition at ~ 12 GPa [4]. It originates from the As-As bonding passing through the Ca layers at first, and then across the K layer with larger ionic radius. Similar structural transitions have been reported in 1144-type $(\text{Cs}, \text{Rb})\text{EuFe}_4\text{As}_4$ with the first collapses of the Eu layers [13]. In summary, the 12442-type hybrid structures $(\text{K}, \text{Rb}, \text{Cs})\text{Ca}_2\text{Fe}_4\text{As}_4\text{F}_2$ are good candidates to explore new structures and high- T_c SCs by pressure.

High pressure is a clean method to manipulate crystal structure and electronic properties of materials without introducing any disorder and impurity. It shortens bond distances and affects electron correlations and band structures. The evolution of T_c as a function of pressure and the related parameters can provide valuable information on the underlying mechanism. In this paper, we report the hydrostatic pressure effect of the 12442-type hole-doped $\text{KCa}_2\text{Fe}_4\text{As}_4\text{F}_2$ studied by electrical transport and x-ray diffraction up to 15 GPa. T_c increases from ~ 33.5 K at ambient pressure to ~ 36.5 K at 2 GPa and shows a slope change around 8 GPa. A crossover from non-Fermi-liquid to Fermi-liquid behavior was also revealed.

High-quality $\text{KCa}_2\text{Fe}_4\text{As}_4\text{F}_2$ samples were prepared via solid-state reaction as described previously [2]. Magnetic properties are measured in a piston cylinder cell up to 1.25 GPa on the commercialized superconducting quantum interference device. Bulk Pb is used as the pressure manometer and glycerol is used as the pressure transmitting medium (PTM). Glycerol is an isotropic liquid and hydrostatic pressure can be retained in the present pressure range. Electrical resistivity under pressure is performed by four-probe method in a cubic anvil pressure cell, which generates much higher hydrostatic pressures up to 15 GPa with multiple-anvil geometry [21]. MgO and pyrophyllite cubes are used as gasket and glycerol is used as PTM. Two samples, 1 and 2, are measured in a ^4He refrigerated chamber ($1.9 \leq T \leq 300$ K).

Figure 1 shows temperature dependence of resistivity $\rho(T)$ of $\text{KCa}_2\text{Fe}_4\text{As}_4\text{F}_2$ under various pressures. $\rho(T)$ appears as metallic behavior with positive temperature coefficients. Moreover, a gradual change in the slope of $\rho(T)$ appears in the high-temperature region, which is generally regarded as the coherence-incoherence crossover in the heavily hole-doped FeSCs [2]. In this paper, we estimated this characteristic temperature T^* by the intersection of two lines across the experimental data as shown in Fig. 1S in Supplemental Material [22]. At AP, T^* is about 150 K. In references, this crossover is usually proposed to describe the interactions between itinerant electrons and local magnetic moments and is accompanied by the changes in magnetic susceptibility [23,24]. As shown in Fig. 1, resistivity decreases linearly on

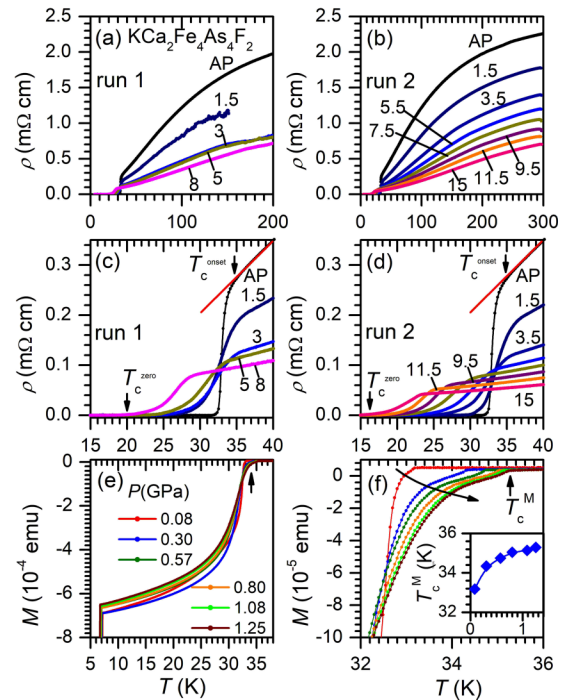


FIG. 1. (a, b) Temperature dependence of resistivity $\rho(T)$ for (a) run 1 up to 8.0 GPa and (b) run 2 up to 15 GPa. (c, d) The enlargement of low- T $\rho(T)$ for (c) run 1 and (d) run 2. The arrows in Figs. 1(c)–1(f) denote the superconducting transition temperatures T_c^{onset} and T_c^{zero} , respectively. (e, f) Magnetic susceptibility $M(T)$ under zero-field cooling process at a magnetic field of $H = 10$ Oe: (e) $M(T)$ curves and (f) the enlargement of $M(T)$ curves near T_c . The inset in panel (f) shows the superconducting transition temperatures T_c^M as a function of pressure. The arrows in panels (c)–(f) represent the T_c^M and its variation trends with pressure.

cooling from ~ 100 K and enters into the superconducting state. The superconducting transition is marked by T_c^{onset} and T_c^{zero} , which are defined as the temperatures where resistivity departs from the linear behavior and reaches zero, respectively [Figs. 1(c) and 1(d)]. At AP, $T_c^{\text{onset}}(T_c^{\text{zero}})$ is ~ 33.5 K (~ 32.2 K), basically consistent with previous reports [2,18]. The application of pressure reduces substantially the room-temperature resistivity at 15 GPa, reaching nearly 1/3 of that at AP. $\rho(T)$ shows gradual decrease for each run without sample dependence in Figs. 1(a) and 1(b). As seen in the enlarged view of low-temperature $\rho(T)$ in Figs. 1(c) and 1(d), the superconducting transition broadens as the pressure increases. Pressure dependences of $\rho(T_c)$, T_c^{onset} , T_c^{zero} , $\Delta T (= T_c^{\text{onset}} - T_c^{\text{zero}})$, and T^* are summarized in Figs. 2(b)–2(e) together with those of $(\text{K}, \text{Rb}, \text{Cs})\text{Ca}_2\text{Fe}_4\text{As}_4\text{F}_2$ at AP for comparison. As the pressure increases, the coherence-incoherence crossover temperature T^* shifts to higher temperatures, reaching ~ 235 K at 15 GPa. Similar behaviors have been observed in other FeAs-based materials [23,24], reflecting the fact that high pressure broadens the bandwidth and enhances the electronic itinerancy [25]. We investigate possible structural changes by examining the resistivity at fixed temperatures as a function of pressure. Usually, structural transformation can affect magnetic interactions and the electronic density of states near the Fermi level, and thus can be

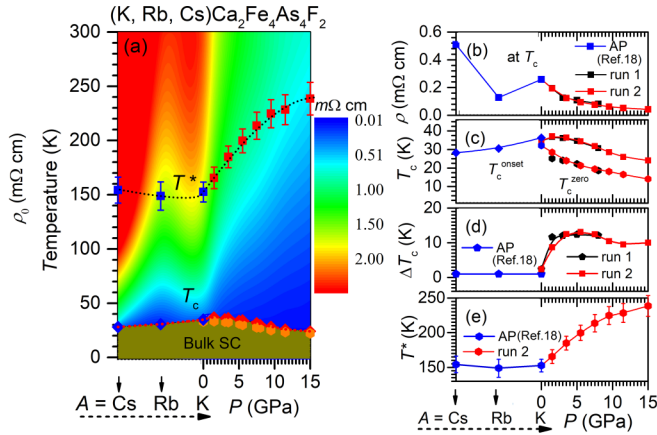


FIG. 2. (a) Temperature-pressure phase diagram of $(\text{K, Rb, Cs})\text{Ca}_2\text{Fe}_4\text{As}_4\text{F}_2$ and $\text{KCa}_2\text{Fe}_4\text{As}_4\text{F}_2$ under pressure; the changing colors describe the evolution of resistivity with pressure. (b–e) Pressure dependence of parameters for $(\text{K, Rb, Cs})\text{Ca}_2\text{Fe}_4\text{As}_4\text{F}_2$: (b) $\rho(T_c)$, (c) T_c^{onset} and T_c^{zero} , (d) ΔT_c (defined as the difference of T_c^{onset} and T_c^{zero}), and (e) the value of T^* to describe the coherence-incoherence crossover.

reflected as a change of resistivity. For example, the pressure-induced collapse and half collapse of tetragonal structures have been identified as the jump of resistivity in KFe_2As_2 and $\text{KCaFe}_4\text{As}_4$, respectively [4,26]. In $\text{KCa}_2\text{Fe}_4\text{As}_4\text{F}_2$, resistivity with pressure at various temperatures [Figs. 3(a) and 3(b)] shows a smooth decrease as a function of pressure without obvious deviation, implying the absence of structural transition up to 15 GPa. Meanwhile, high-pressure x-ray diffraction was also performed up to 15.86 GPa at room temperature as shown in Fig. 2S in Supplemental Material [22] and the absence of clear splitting or additional diffraction peaks versus pressures further confirmed that there is no pressure-induced half collapse of tetragonal structure below 15 GPa.

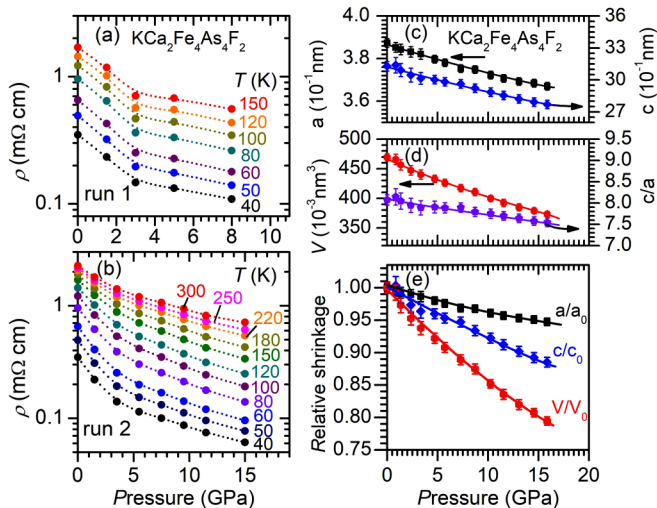


FIG. 3. (a, b) Resistivity vs pressure at various temperatures for (a) run 1 up to 8.0 GPa and (b) run 2 up to 15 GPa. Resistivity decreases smoothly with increasing the pressure without any departures, suggesting no structural transition below 15 GPa. (c–e) Pressure dependence of lattice parameters (a , c , c/a , and V) and the relative shrinkage (a/a_0 , c/c_0 , and V/V_0).

The evolution of T_c is checked further by comparing $M(T)$ curves under zero-field cooling process at a magnetic field of $H = 10$ Oe. Magnetic susceptibility under pressure was measured for $\text{KCa}_2\text{Fe}_4\text{As}_4\text{F}_2$ in a piston cylinder cell. Large magnetic shielding effect below T_c is found as the evidence of bulk superconductivity in Figs. 1(e) and 1(f). The estimated superconducting volume fraction is found to be $\sim 100\%$ by comparing the jump in magnetizations of $\text{KCa}_2\text{Fe}_4\text{As}_4\text{F}_2$ and Pb, consistent with the previous report [2]; the superconducting volume fraction changes insensitively until 1.25 GPa compared to AP. The value of T_c^M increases monotonously from ~ 33.2 K at 0.08 GPa to ~ 35.3 K at 1.25 GPa and tends to saturate with further increasing pressure.

In Fig. 2(a), a temperature-pressure phase diagram is constructed by summarizing these above data and those of $(\text{K, Rb, Cs})\text{Ca}_2\text{Fe}_4\text{As}_4\text{F}_2$ at AP from Ref. [18]. A domelike superconducting phase diagram is revealed with a maximum value of ~ 36.5 K near 2 GPa in the background of enhanced resistivity of $(\text{Rb, Cs})\text{Ca}_2\text{Fe}_4\text{As}_4\text{F}_2$. At AP, superconductivity emerges with larger normal-state residual resistivity, while the residual resistivity at 15 GPa is nearly one order of magnitude smaller than that of AP. The details are given in Fig. 2(b), in which the normal-state resistivity just above T_c , $\rho(T_c)$, shows a gradual decrease as the pressure increases. It can be understood as follows: chemical doping influences band structures by changing electronic density of states at the Fermi energy level and/or shifting the position of the Fermi level, while high pressure can broaden the bandwidth and enhances the itinerancy of electrons. Another reason is the different compression ratios of crystal axes: the chemical pressure from Cs, Rb, and K shortens the c axis more strongly in comparison with the a axis while both crystallographic axes are compressed under physical pressure. As shown in Fig. 2(c), T_c^{onset} is increased from ~ 33.5 K at ambient pressure to ~ 36.5 K near 2 GPa with a slope change near 8 GPa while the T_c^{zero} value decreases. ΔT_c increases gradually and reaches a maximum of ~ 12 K at 6.0 GPa, and then decreases to ~ 10 K at 15 GPa. The stress effect and the enhanced anisotropy under pressure may be the main reasons for the broadening of the superconducting transition.

Temperature dependence of normal-state resistivity in the vicinity of T_c provides important information on the superconducting properties. $\rho(T)$ data of $\text{KCa}_2\text{Fe}_4\text{As}_4\text{F}_2$ at $T < 80$ K are analyzed by fitting with $\rho = \rho_0 + AT^n$ where ρ_0 is the residual resistivity and A and n are the temperature coefficient and the exponent. The value of n shows a gradual increase from $\sim 1.05 \pm 0.1$ at AP to $\sim 1.92 \pm 0.1$ at 15 GPa, indicating the recovery of the Fermi-liquid state by the application of pressure. According to the literature [10,11], $\text{KCa}_2\text{Fe}_4\text{As}_4\text{F}_2$ is a multigap superconductor with strong magnetic fluctuations above T_c that are related to its non-Fermi-liquid behavior. Interestingly, high- T_c SC at lower pressure with an unconventional non-Fermi-liquid state is changed into low- T_c SC at elevated pressures with a Fermi-liquid behavior in the normal state. We noticed that these fittings are too simple to give more information on the multiband effects. In Figs. 4(a) and 4(b), we thus adopt an empirical formula $\rho = \rho_0 + A_1T + A_2T^2$ to construct the relation between the evolution of temperature coefficient and T_c as mentioned earlier [27,28]. All the parameters in Fig. 4 are obtained from the

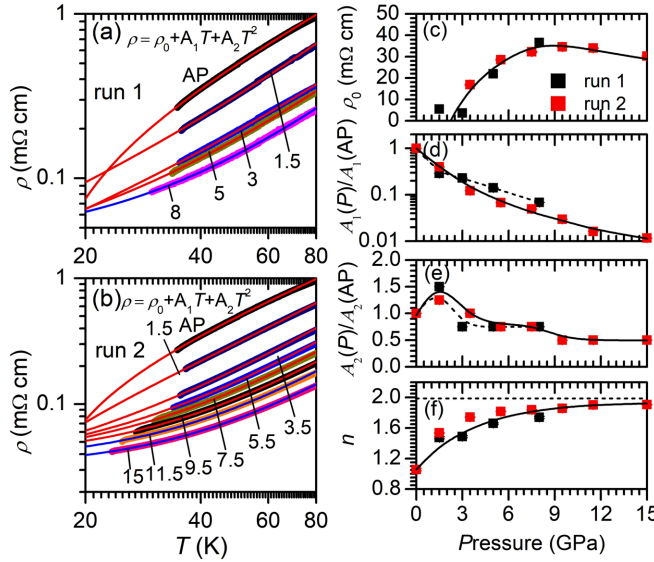


FIG. 4. (a, b) The normal-state $\rho(T)$ just above T_c was analyzed by the formula $\rho = \rho_0 + A_1 T + A_2 T^2$ for (a) run 1 and (b) run 2. ρ_0 represents the residual resistivity and the parameters A , A_1 , and A_2 are the temperature coefficients. To make the results more credible, we describe the relative changes of $A_1(P)/A_1(\text{AP})$ and $A_2(P)/A_2(\text{AP})$ since they are not single crystals. (c–f) Pressure dependence of the related parameters: (c) ρ_0 , (d) exponent n , (e) $A_1(P)/A_1(\text{AP})$ value, and (f) $A_2(P)/A_2(\text{AP})$ value. The solid black lines indicate the changing trends of these parameters.

best fit to experimental data ($T_c < T < 80$ K) as presented in Figs. 4(c)–4(f). The $A_2 T^2$ term describes Fermi liquid and the $A_1 T$ term reflects electronic correlations and scattering, e.g., the electron-boson interaction and/or the critical fluctuations near the QCP. Pressure dependences of these parameters are compared: ρ_0 shows a broad peak around 8.0 GPa, and its enhancement is similar to that of the Co substitution [5]. However, high pressure does not introduce any disorder. In other reports, the increases of ρ_0 can be taken as an evidence for the collapse of tetragonal structure [4,27], which is inconsistent with the above high-pressure structural study. Therefore, the increase of ρ_0 is an evidence for an electronic phase transition. To make the results more credible, we describe the relative changes of $A_1(P)/A_1(\text{AP})$ and $A_2(P)/A_2(\text{AP})$ since they are not single crystals. As the pressure increases, the value of $A_1(P)/A_1(\text{AP})$ decreases linearly by nearly two orders of magnitude compared to AP, coinciding with the suppression of T_c . This observation implies that the T -linear term plays an important role in gluing the superconducting pairings. Thus, the resulting overall trend of change is that the value of T_c decreases gradually with increasing pressure. Meanwhile, the $A_2(P)/A_2(\text{AP})$ shows an enhancement near 2 GPa, which matches perfectly with the peak value of T_c as presented in Fig. 2(a). As mentioned above, the $A_2(P)/A_2(\text{AP})$ is usually proportional to the square of the Sommerfeld coefficient via the Kadowaki-Woods relationship, and a measure of density of states at Fermi level $N(E_F)$; thus, the enhanced T_c near 2 GPa is attributed to the increasing value of $N(E_F)$ by pressure. With further increasing pressure, the $A_2(P)/A_2(\text{AP})$ value shows an increasing trend near 8 GPa, which is re-

sponsible for the slope change of T_c . Considering its multi-gap characteristic, other factors such as pressure variation of phonon models may affect T_c and its pressure dependence. The combined interplay of these factors would be important to fully understand the evolution of T_c with pressure.

Finally, we discuss the evolution of T_c with pressure in $\text{KCa}_2\text{Fe}_4\text{As}_4\text{F}_2$. As mentioned above, the enhancement of T_c near 2 GPa correlates with the increasing values of $A_2(P)/A_2(\text{AP})$ and $N(E_F)$ according to the Kadowaki-Woods relationship. A likely reason of this phenomenon is different compression ratios of KFe_2As_2 units and CaFeAsF blocks by pressure, which result in charge redistributions. The self-doping is possible and requires further verifications of the Fe valence state. According to the pressure dependence of lattice parameters in Figs. 3(c)–3(e) and the reported ones of $(\text{Cs, Rb, K})\text{Fe}_2\text{As}_2$ [18,26,29], the alkali-metal element substitution and high pressure are summarized: with increasing the substitution from Cs, Rb, and K, lattice parameters a , c , and c/a and the volume V decrease by about -0.41 , -3.7 , -3.2 , and -4.2% , respectively, while a , c , c/a , and V at 15.86 GPa reduce by -5.2 , -11.5 , -6.6 , and -20.5% compared to those at AP, implying the anisotropic contraction. Considering that the double Fe_2As_2 layers are the dominating contributions of critical fluctuations, the charge redistributions can be responses for pressure-induced crossover from non-Fermi-liquid ($n \sim 1.05 \pm 0.1$ at AP) to Fermi-liquid behavior ($n \sim 1.92 \pm 0.1$ at 15 GPa) [2,6]. Moreover, T_c decreases with increasing the pressure and is accompanied by the increasing T^* , which is consistent with the case in the pressurized KFe_2As_2 [25], while T_c enhances with the increase of T^* in $(\text{Cs, Rb, K})\text{Fe}_2\text{As}_2$ at ambient pressure [23–25]. It implies that this relationship is not universal and depends on detailed systems. The second question is why there is no half-collapsed tetragonal transition in $\text{KCa}_2\text{Fe}_4\text{As}_4\text{F}_2$. Theoretical calculations have predicted that critical pressure of half-collapsed tetragonal transition increases with the larger cation radius KFe_2As_2 [30]. For example, both $\text{KCaFe}_4\text{As}_4$ and $(\text{Rb, Cs})\text{EuFe}_4\text{As}_4$ undergo half-collapsed tetragonal transition with the As-As bonding across the Ca layers at ~ 4 GPa ($\text{Ca}^{2+} \sim 1.0 \text{ \AA}$) [4] and the Eu layers at ~ 10 and ~ 12 GPa ($\text{Eu}^{2+} \sim 1.2 \text{ \AA}$) [13], and then collapsed tetragonal transition with As-As bonding across the K layer at ~ 11 GPa ($\text{K}^+ \sim 1.4 \text{ \AA}$), the Rb layer at ~ 20 GPa ($\text{Rb}^+ \sim 1.5 \text{ \AA}$), and the Cs layer at ~ 30 GPa ($\text{Cs}^+ \sim 1.7 \text{ \AA}$). For $\text{KCa}_2\text{Fe}_4\text{As}_4\text{F}_2$ [2,18], the thick Ca_2F_2 layer separates the nearest As-As bonding and complete collapse of tetragonal structure cannot be formed. The most likely possibility is to form half-collapsed tetragonal structure with As-As bonding across K layers ($\text{K}^+ \sim 1.4 \text{ \AA}$) in KFe_2As_2 blocks. According to structural analysis of KFe_2As_2 [26], pressured-induced collapse of tetragonal structure appears at ~ 16 GPa, indicating that critical pressure of $\text{KCa}_2\text{Fe}_4\text{As}_4\text{F}_2$ is higher than ~ 16 GPa. Third, although the dome-like superconducting phase diagrams are similar for alkali-metal element substitutions (from Cs, Rb, and K) and hydrostatic pressure up to 15 GPa, they affect the superconducting state in different manners. As shown in Figs. 3(c)–3(e), the element substitutions (from Cs, Rb, and K) shorten the c axis ($\sim -3.7\%$) more quickly than they shorten the a axis ($\sim -0.41\%$); the contraction at 15.86 GPa compared to AP is ~ -11.5 and

$\sim -5.2\%$ for the c axis and the a axis, respectively; the normalization results show that the a axis shrinks faster compared to the c axis under hydrostatic pressure, which is different from the element substitution (from Cs, Rb, and K). To understand this scenario, evolutions of band structures are required.

In summary, hydrostatic pressure effect on the normal and superconducting states of $\text{KCa}_2\text{Fe}_4\text{As}_4\text{F}_2$ has been investigated. T_c increases from ~ 33.5 K at ambient pressure to ~ 36.5 K near 2 GPa with a slope change around 8 GPa. The value of T_c is found to be inversely proportional to the characteristic temperature of the coherence-incoherence crossover. Both electrical resistivity versus temperatures/pressures and high-pressure x-ray diffraction suggest the absence of a pressure-induced half-collapsed tetragonal phase below

15 GPa. Pressure-induced crossover from non-Fermi-liquid (the exponent $n \sim 1.05 \pm 0.1$ at ambient pressure) to Fermi-liquid behavior ($n \sim 1.92 \pm 0.1$ at 15 GPa) was revealed.

We thank S. Nagasaki and Dr. Gouchi for technical assistance. This work is supported by the National Key Research and Development Program of China (Grants No. 2018YFA0305700 and No. 2018YFA0305800), the Strategic Priority Research Program and Key Research Program of Frontier Sciences of the Chinese Academy of Sciences (CAS Grants No. XDB07020100 and No. QYZDB-SSW-SLH013), National Natural Science Foundation of China (Grant No. 11574377), IOP Hundred-Talent Program (Grant No. Y7K5031X61), Youth Promotion Association, and CAS (Grant No. 2018010).

-
- [1] A. Iyo, K. Kawashima, T. Kinjo, T. Nishio, S. Ishida, H. Fujihisa, Y. Gotoh, K. Kihou, H. Eisaki, and Y. Yoshida, *J. Am. Chem. Soc.* **138**, 3410 (2016).
- [2] Z.-C. Wang, C.-Y. He, S.-Q. Wu, Z. T. Tang, Y. Liu, A. Ablimit, C.-M. Feng, and G.-H. Cao, *J. Am. Chem. Soc.* **138**, 7856 (2016).
- [3] Y. Liu, Y. B. Liu, Z. T. Tang, H. Jiang, Z.-C. Wang, A. Ablimit, W. H. Jiao, Q. Tao, C.-M. Feng, Z.-A. Xu, and G.-H. Cao, *Phys. Rev. B* **93**, 214503 (2016).
- [4] U. S. Kaluarachchi, V. Taufour, A. Sapkota, V. Borisov, T. Kong, W. R. Meier, K. Kothapalli, B. G. Ueland, A. Kreyssig, R. Valenti, R. J. McQueeney, A. I. Goldman, S. L. Budko, and P. C. Canfield, *Phys. Rev. B* **96**, 140501(R) (2017).
- [5] J. Ishida, S. Iimura, and H. Hosono, *Phys. Rev. B* **96**, 174522 (2017).
- [6] G. T. Wang, Z. W. Wang, and X. B. Shi, *Europhys. Lett* **116**, 37003 (2016).
- [7] A. Iyo, K. Kawashima, S. Ishida, H. Fujihisa, Y. Gotoh, H. Eisaki, and Y. Yoshida, *J. Am. Chem. Soc.* **140**, 369 (2018).
- [8] J.-K. Bao, K. Willa, M. P. Smylie, H. J. Chen, U. Welp, D. Y. Chung, and M. G. Kanatzidis, *Cryst. Growth Des.* **18**, 3517 (2018).
- [9] K. Cho, A. Fente, S. Teknowijoyo, M. A. Tanatar, K. R. Joshi, N. M. Nusran, T. Kong, W. R. Meier, U. Kaluarachchi, I. Guillamon, H. Suderow, S. L. Budko, P. C. Canfield, and R. Prozorov, *Phys. Rev. B* **95**, 100502 (R) (2017).
- [10] F. K. K. Kirschner, D. T. Adroja, Z.-C. Wang, F. Lang, M. Smidman, P. J. Baker, G.-H. Cao, and S. J. Blundell, *Phys. Rev. B* **97**, 060506(R) (2018); D. T. Adroja, F. K. K. Kirschner, F. Lang, M. Smidman, A. D. Hillier, Z.-C. Wang, G.-H. Cao, G. B. G. Stenning, and S. J. Blundell, *J. Phys. Soc. Jpn.* **87**, 124705 (2018).
- [11] R. Yang, Y. M. Dai, B. Xu, W. Zhang, Z. Y. Qiu, Q. T. Sui, C. C. Homes, and X. G. Qiu, *Phys. Rev. B* **95**, 064506 (2017).
- [12] Q.-P. Ding, W. R. Meier, A. E. Bohmer, S. L. Budko, P. C. Canfield, and Y. Furukawa, *Phys. Rev. B* **96**, 220510(R) (2017).
- [13] D. E. Jackson, D. VanGennep, W. Bi, D. Z. Zhang, P. Materne, Y. Liu, G.-H. Cao, S. T. Weir, Y. K. Vohra, and J. J. Hamlin, *Phys. Rev. B* **98**, 014518 (2018).
- [14] M. P. Smylie, K. Willa, J.-K. Bao, K. Ryan, Z. Islan, H. Claus, Y. Simsek, Z. Diao, A. Rydh, A. E. Koshelev, W.-K. Kwok, D. Y. Chung, M. G. Kanatzidis, and U. Welp, *Phys. Rev. B* **98**, 104503 (2018).
- [15] Z.-C. Wang, C.-Y. He, S.-Q. Wu, Z.-T. Tang, Y. Liu, A. Ablimit, Q. Tao, C.-M. Feng, Z.-A. Xu, and G.-H. Cao, *J. Phys.: Condens. Matter* **29**, 11LT01 (2017).
- [16] W. R. Meier, Q.-P. Ding, A. Kreyssig, S. L. Bud'ko, A. Sapkota, K. Kothapalli, V. Borisov, R. Valenti, C. D. Batista, P. P. Orth, R. M. Fernandes, A. I. Goldman, Y. Furukawa, A. E. Böhrer, and P. C. Canfield, *npj Quantum Mater.* **3**, 5 (2018).
- [17] S. Yang, W. L. You, S. J. Gu, and H. Q. Lin, *Chin. Phys. Soc.* **18**, 1674 (2009).
- [18] Z.-C. Wang, C. Y. He, Z. T. Tang, S. Q. Wu, and G.-H. Cao, *Sci. China Mater.* **60**, 83 (2017).
- [19] Z.-C. Wang, C. Y. He, S. Q. Wu, Z. T. Tang, Y. Liu, and G.-H. Cao, *Chem. Mater.* **29**, 1805 (2017).
- [20] S. Q. Wu, Z.-C. Wang, C.-Y. He, Z.-T. Tang, Y. Liu, and G.-H. Cao, *Phys. Rev. Mater.* **1**, 044804 (2017).
- [21] N. Mori, H. Takahashi, and N. Takeshita, *High Pressure Res.* **24**, 225 (2004).
- [22] See Supplemental Material at <http://link.aps.org/supplemental/10.1103/PhysRevB.99.014501> for the summary of electrical transport at ambient pressure and high pressures and high-pressure x-ray diffraction.
- [23] F. Hardy, A. E. Bohmer, D. Aoki, P. Burger, T. Wolf, P. Schweiss, R. Heid, P. Adelmann, Y. X. Yao, G. Kotliar, J. Schmalian, and C. Meingast, *Phys. Rev. Lett.* **111**, 027002 (2013).
- [24] Y. P. Wu, D. Zhao, A. F. Wang, N. Z. Wang, Z. J. Xiang, X. G. Luo, T. Wu, and X. H. Chen, *Phys. Rev. Lett* **116**, 147001 (2016).
- [25] P. Wiecki, V. Taufour, D. Y. Chung, M. G. Kanatzidis, S. L. Budko, P. C. Canfield, and Y. Furukawa, *Phys. Rev. B* **97**, 064509 (2018).
- [26] Y. Nakajima, R. X. Wang, T. Metz, X. F. Wang, L. M. Wang, H. Cynn, S. T. Weir, J. R. Jeffries, and J. Paglione, *Phys. Rev. B* **91**, 060508(R) (2015).
- [27] M. Nakajima, S. Ishida, T. Tanaka, K. Kihou, Y. Tomioka, T. Saito, C. H. Lee, H. Fukazawa, Y. Kohori, T. Kakeshita, A. Iyo, T. Ito, H. Eisaki, and S. Uchida, *Sci. Rep.* **4**, 5873 (2014).

- [28] R. A. Cooper, Y. Wang, B. Vignolle, O. J. Lipscombe, S. M. Hayden, Y. Tanabe, T. Adachi, Y. Koike, M. Nohara, H. Takagi, C. Proust, and N. E. Hussey, *Science* **323**, 603 (2009).
- [29] S. K. Mishra, R. Mittal, S. L. Chaplot, S. V. Ovsyannikov, D. M. Trots, L. Dubrovinsky, Y. Su, Th. Brueckel, S. Matsuishi, H. Hosono, and G. Garbarino, *Phys. Rev. B* **84**, 224513 (2011).
- [30] Z. Yu, L. Wang, L. Wang, H. Liu, J. Zhao, C. Li, S. Sinogeikin, W. Wu, J. Luo, N. Wang, K. Yang, Y. Zhao, and H.-K. Mao, *Sci. Rep.* **4**, 7172 (2014).